Neuroprotective effect of Ginsenoside Re against neurotoxin-induced Parkinson's disease models via induction of Nrf2

JUHUI QIAO*, YUCHU ZHAO*, YING LIU, SIYU ZHANG, WENXUE ZHAO, SHICHAO LIU and MEICHEN LIU

Jilin Ginseng Academy, Changchun University of Chinese Medicine, Changchun, Jilin 130117, P.R. China

Received January 3, 2022; Accepted April 12, 2022

DOI: 10.3892/mmr.2022.12731

Abstract. The aim of the present study was to examine the neuroprotective effects of a panel of active components of ginseng and to explore their molecular mechanisms of action in two rotenone (Rot)-induced models of Parkinson's disease: An *in vitro* model using the human neuroblastoma cell line SH-SY5Y and an *in vivo* model using *Drosophila*. Ginsenoside Re (Re) was identified as the most potent inhibitor of Rot-induced cytotoxicity in SH-SY5Y cells by Cell Counting kit-8 assay and lactate dehydrogenase release assay. Flow cytometry, Hoechst staining, Rhodamine 123 staining, ATP and cytochrome c release revealed that Re rescue of Rot-induced mitochondrial dysfunction and inhibition of the mitochondrial apoptotic pathway. Western blot analysis demonstrated that Re alleviated Rot-induced oxidative stress by activating the nuclear factor erythroid 2-related factor 2 (Nrf2) anti-oxidant pathway, and these effects were abolished by RNA interference-mediated knockdown of Nrf2. Re enhanced phosphorylation of components of the phosphatidylinositol 3-kinase (PI3K)/protein kinase B (AKT) and extracellular regulated protein kinase (ERK) pathways, and pharmacological inhibition of these pathways reduced Re-mediated Nrf2 activation and neuroprotection. In the *Drosophila* model, Immunofluorescence microscopy, reactive oxygen species (ROS), hydrogen peroxide and knockdown analysis revealed that Re reversed Rot-induced motor deficits and dopaminergic neuron loss while concomitantly alleviating Rot-induced oxidative damage. The findings of the present study suggest that Re protects neurons against Rot-induced mitochondrial dysfunction and oxidative damage, at least in part, by inducing Nrf2/heme oxygenase-1 expression and activation of the dual PI3K/AKT and ERK pathways.

Correspondence to: Dr Shichao Liu or Professor Meichen Liu, Jilin Ginseng Academy, Changchun University of Chinese Medicine, 1035 Boshuo Road, Nanguan, Changchun, Jilin 130117, P.R. China
E-mail: aralekyra@163.com
E-mail: liumc0367@163.com

*Contributed equally

Key words: Parkinson's disease, rotenone, ginseng, mitochondrial dysfunction, oxidative stress

Introduction

Parkinson's disease (PD) and Alzheimer's disease are the most prevalent degenerative neurological disorders (1). As the aging population in most countries increases, the incidence of PD is expected to surge, posing a considerable personal and economic burden on families and the larger society (2). The main pathological features of PD are progressive loss of dopaminergic (DA) neurons and decreased dopamine levels (3). To date, the compound l-dopa is considered as the optimal treatment for PD in clinical practice; however, long-term use of this compound causes complications such as efficacy attenuation, motor fluctuation, and dysmotility, and it cannot prevent or delay disease progression (4). Therefore, there is an urgent need to understand the pathogenesis of PD in greater detail in order to facilitate the search for new safe and effective drugs that can delay disease progression.

The pathogenesis of PD is complex, involving misfolding and abnormal aggregation of α-synuclein (α-syn), oxidative stress, and mitochondrial dysfunction (5). DA neurons have high oxygen consumption and metabolic rates and generate large quantities of reactive oxygen species (ROS) that can damage mitochondria. Analysis of the brains of PD patients at autopsy have shown that the activity of mitochondrial complex I (the main site of ROS generation) in the substantia nigra is selectively decreased and mitochondrial function is impaired, suggesting that oxidative stress and mitochondrial dysfunction play a key role in the selective destruction of DA neurons (6). Additional studies have shown that oxidative stress and mitochondrial dysfunction can induce α-syn to form soluble oligomers, which then undergo misfolding to form insoluble fibers (7-9). In turn, abnormal aggregation of α-syn can amplify oxidative stress and mitochondrial dysfunction, creating a vicious cycle that eventually triggers degeneration of DA neurons in the substantia nigra. Therapeutic agents that reduce ROS levels may maintain mitochondrial function and break the destructive cycle of events, thereby delaying the loss of DA neurons in PD.

Activation of apoptosis can occur through various mechanisms, including via the phosphatidylinositol 3-kinase

(PI3K)/protein kinase B (AKT) and extracellular regulated protein kinase (ERK) signaling pathways, which also play important roles in cell proliferation and differentiation (10). Previous studies have found that the PI3K/AKT and ERK pathways are associated with and may activate the downstream transcription factor nuclear factor erythroid 2-related factor 2 (Nrf2), leading to expression of its antioxidant target gene heme oxygenase-1 (HO-1) (11-13). Therefore, drugs that regulate these pathways and protect from oxidative stress-induced apoptosis may have neuroprotective activity.

Panax ginseng C.A. Meyer is a traditional herbal medicine in China and has been demonstrated to have numerous pharmacological effects on the nervous system (14). The antioxidant and neuroprotective properties are mediated by ginsenosides, the main active ingredients in ginseng. In particular, these properties have been demonstrated for ginsenoside Re (Re) in a variety of neurodegenerative disease models *in vivo* and *in vitro (*15). However, the mechanism of action of Re in PD remains unclear.

Rotenone (Rot), a naturally occurring isoflavone that inhibits the mitochondrial electron transport chain complex I, is commonly used to model PD by virtue of its ability to reproduce numerous features of PD in animal models. Moreover, epidemiological studies have shown that chronic exposure of individuals to Rot confers an increased risk for PD (16). In the present study, the effects of Re on Rot-induced PD models *in vitro* and *in vivo* were analyzed and it was established that Re had potent neuroprotective effects. The molecular mechanism of Re-mediated neuroprotection was further examined and it was determined that it acts by countering oxidative stress and maintaining mitochondrial function. The results of the present study, thus lay the foundation for further development of traditional Chinese medicines as treatments to prevent or delay PD.

Materials and methods

Drugs. The ginsenosides Re, Rg1, Rg2, Rg3 and Rh2 (monomeric compounds identified by HPLC method, purity ≥98%; batch nos. DSTDR001401, DSTDR000901, DSTDR001001, DSTDR001101 and DSTDS003601) were all purchased from Chengdu Desite Biological Technology Co., Ltd. All drugs were dissolved in dimethyl sulfoxide (DMSO), and each experimental and control group contained ≤0.1%v/v DMSO.

Cell culture. SH-SY5Y cells were obtained from the American Type Culture Collection (cat. no. CRL-2266) and cultured in DMEM/F12 complete medium (supplemented with 10% fetal bovine serum and 1% penicillin-streptomycin; all from Hyclone; Cytiva) at 37˚C in a 5% CO_2 atmosphere.

Cell Counting Kit-8 (CCK-8) cell viability assay. Cell viability was analyzed using a CCK-8 assay kit (Boster Biological Technology) according to the manufacturer's instructions. SH-SY5Y cells were seeded in 96-well plates ($3x10^3$ cells/well) and incubated at 37˚C for 24 h. The cells were then co-treated with 0.3 μM Rot (Dalian Meilun Biotechnology Co., Ltd.; cat. no. MB5842) and Re (1, 2.5, 5, or 10 μM), Rg1 (2.5 μM), Rg2 (5 μM), Rg3 (10 μM), Rh2 (10 μM), or L-dopamine (Beijing Solarbio Science & Technology Co., Ltd.; cat. no. ID0360; 5 or 10 μM) for 24 h. CCK-8 solution was added at 20 μl/well and the plates were incubated in the dark at 37˚C for 30 min. The absorbance at 450 nm was measured with a microplate reader (Tecan Group, Ltd.).

Lactate dehydrogenase (LDH) release assay. LDH was measured using an LDH cytotoxicity assay kit (Nanjing Jiancheng Bioengineering Institute; cat. no. A020-2-2) according to the manufacturer's guidelines. Cells were seeded at $5x10^4$ cells/well and co-treated with Re (1, 2.5, 5, or 10 μM) and Rot (0.3 μM) at 37˚C for 24 h. The absorbance at 490 nm was then measured with a microplate reader (Tecan Group, Ltd.) at room temperature.

Apoptosis assay. Cells undergoing apoptosis were detected by flow cytometry after staining with Annexin V-FITC and PI (Becton Dickinson and Company). Cells were seeded at $5x10^4$ cells/well and co-treated with Rot (0.3 μM) and Re (5 μM) at 37˚C for 24 h. The cells were collected, washed twice with phosphate-buffered saline (PBS), resuspended in 1X Binding Buffer, and mixed with Annexin V-FITC and PI staining solution. The cells were incubated at room temperature in the dark for 15 min and then analyzed using an flow cytometer (Amnis Corporation), and quantified using IDEAS software v6.1 (Amnis Corporation).

Fluorescence microscopy. Cells were seeded at $5x10^4$ cells/well and co-treated with Rot (0.3 μM) and Re (5 μM) at 37˚C for 24 h. The cells were then fixed in 4% paraformaldehyde (PFA) solution for 0.5 h at room temperature, washed twice with PBS, and incubated with Hoechst 33342 (Beyotime Institute of Biotechnology) staining solution at 1 ml/well. The plates were incubated at 37˚C in the dark for 30 min, washed twice with PBS, and visualized using with an EVOS fluorescence microscope (Thermo Fisher Scientific, Inc.).

Caspase assay. Caspase activities were measured using Caspase-3, Caspase-8 and Caspase-9 (cat nos. C1115, C1151; C1157; Beyotime Institute of Biotechnology) Activity assay kits according to the manufacturers' instructions. Cells were washed with PBS, centrifuged at 4˚C (530 x g, 5 min) and 100 μl lysate was used per $2x10^5$ cells and incubated on ice for 15 min. Centrifugation at 4,246 x g at 4˚C for 10 min. Protein concentration in supernatant was measured using a Bradford assay kit (Tiangen Biotech Co., Ltd.). Then 50 μl cell lysate supernatant and 10 μl AC-DevD-PNA (2 mM) for caspase-3, AC-IETD-PNA (2 mM) for caspase-8 and AC-LEHD -pNA (2 mM) for caspase-9 was mixed in a 40 μl detection buffer at 37˚C for 4 h and then analyzed using a microplate reader (Tecan Group, Ltd.).

Detection of adenosine triphosphate (ATP) content. ATP was measured using a chemiluminescence ATP assay kit (Beyotime Institute of Biotechnology; cat. no. S0026). Following incubation of SH-SY5Y cells ($5x10^4$ cells/well) with Rot (0.3 μM) and Re (5 μM) at 37˚C for 24 h, the medium was discarded, 200 μl of ATP detection solution was added, and the plates were centrifuged at 4,246 x g for 5 min at 4˚C. The supernatant was transferred to a new tube. A total of 100 μl of ATP detection buffer was added to each assay well and incubate at 37˚C for 3 min to deplete background, followed by addition of 20 μl

of supernatant to the assay wells. Optical density values were recorded using a microplate reader (Tecan Group, Ltd.) and ATP content was converted according to a standard curve.

Mitochondrial membrane potential (MMP) analysis by fluorescence microscopy. Cells were seeded at $5x10^4$ cells/well and were incubated with Rot (0.3 μM) with or without Re (5 μM) at 37˚C for 24 h, washed twice with PBS, mixed with 1 ml of JC-1 solution (Beijing Solarbio Science & Technology Co., Ltd.; cat. no. J8030) and incubated in the dark for 20 min (maintained at 37˚C). The cells were washed twice with JC-1 staining buffer. The cells were then processed and examined with an EVOS fluorescence microscope (Thermo Fisher Scientific, Inc.).

MMP analysis by flow cytometry. Cells were seeded at $5x10^4$ cells/well and were incubated with Rot (0.3 μM) with or without Re (5 μM) at 37˚C for 24 h, washed twice with PBS, mixed with Rhodamine 123 (2 μM) (Beijing Solarbio Science & Technology Co., Ltd.; cat. no. R8030), and incubated at 37˚C for 30 min in the dark. The cells were then centrifuged at 530 x g for 5 min at room temperature, resuspended in PBS, and analyzed using a flow cytometer (Amnis Corporation), and quantified using IDEAS software v6.1 (Amnis Corporation).

Intracellular ROS assay. Intracellular ROS levels were detected by flow cytometry (Amnis Corporation) and quantified using IDEAS software v6.1 (Amnis Corporation) or fluorescence microplate reader. Cells were seeded at $5x10^4$ cells/well and were incubated with Rot (0.3 μM) and Re (5 μM) at 37˚C for 24 h, washed twice with PBS, mixed with 100 μl of 2,7-dichlorofluorescein diacetate (DCFH-DA; Beijing Solarbio Science & Technology Co., Ltd.; cat. no. CA1410) diluted in serum-free DMEM/F12 medium (final concentration, 10 μM), and incubated in the dark for 20 min at 37˚C. The cells were then centrifuged at 530 x g for 5 min at room temperature, resuspended in PBS, and analyzed using an Amnis® flow cytometer. Alternatively, cells were seeded at $3x10^3$ cells/well and incubated with Rot (0.3 μM) and Re (5 μM) at 37˚C for 24 h, after being washed by PBS were inoculated into black 96-well plates, and a 10-μl probe was added before detection. The cells were incubated at 37˚C for 20 min under dark conditions, and then detected using a fluorescence microplate reader. The excitation wavelength was 488 nm, and the emission wavelength was 530 nm.

Oxidative stress marker assays. Cells were seeded at $5x10^4$ cells/well and incubated with Rot (0.3 μM) in the presence or absence of Re (5 μM) at 37˚C for 24 h. Glutathione (GSH), malondialdehyde (MDA), superoxide dismutase (SOD), and glutathione peroxidase (GSH-Px) were assayed using kits (Nanjing Jiancheng Bioengineering Institute; cat. no. A006-2-1, A003-4-1, A001-3-2, A005-1-2) according to the manufacturer's instructions and measured with a microplate reader (Tecan Group, Ltd.).

Inhibitor treatment and small interfering RNA (siRNA) transfection. Experiments involving the following inhibitors included cell viability, ROS detection and western blotting: 15 μM PD98059 (ERK1/2 signal inhibitor, cat. no. HY-12028), 15 μM LY294002 (PI3K/AKT inhibitor, cat. no. HY-10108), 5 μM Akt inhibitor IV (cat. no. HY14971). 5 μM SB203580 [p38 mitogen-activated protein kinase (MAPK) inhibitor, cat. no. HY10256], 10 μM SP600125 [Jun N-terminal kinase (JNK) inhibitor, cat. no. HY12041], and 10 μM Compound C [CC; Adenosine 5'-monophosphate (AMP)-activated protein kinase (AMPK) inhibitor, cat. no. HY13418A], were only used in cell viability assays to determine which signalling pathways mediate Nrf2 activation. The inhibitors were added to cells before Re and/or Rot treatment for 1 h at 37˚C and all inhibitors were purchased from Med Chem Express corporation. A customized siRNA reagent system (Guangzhou RiboBio Co., Ltd.) was used for cell viability or ROS assays as previously described (17). The target sequence of the negative control for RNA interference was 5'-CGUACGCGGAAUACUUCGA-3' and the interference target sequences for Nrf2 were as follows: NRF2 siRNA-1, 5'-GAATGGTCCTAAAACACCA-3'; NRF2 siRNA-2; 5'-GAGAAAGAATTGCCTGTAA-3'; and NRF2 siRNA-3, 5'-GCTACGTGATGAAGATGGA-3'.

Western blot analysis. Cells were washed twice with PBS and centrifuged at 530 x g at 4˚C to obtain cells pellet, cells were lysed with RIPA lysis buffer (Beyotime Institute of Biotechnology) and total protein was measured using a BCA kit (Beijing Solarbio Science & Technology Co., Ltd.; cat. no. P0012S). Subcellular fractions were produced using a Cell Mitochondria Isolation Kit (Beyotime Institute of Biotechnology; cat. no. C3601) for cytosolic and mitochondrial fractions and a Nuclear and Cytoplasmic Protein Extraction Kit (Beyotime Institute of Biotechnology; cat. no. P0027) for nuclear and cytosolic fractions. Proteins (20 μg/lane) were separated by SDS-PAGE and electron transfer onto a nitrocellulose membrane. Non-specific protein binding was blocked by incubation of the membranes with 5% (v/v) non-fat dried milk in PBS for 1 h at 25˚C and the membranes were incubated overnight at 4˚C with anti-B-cell lymphoma-2 (Bcl-2; 1:1,000; cat. no. BS1511), anti-Bcl-2 associated X protein (Bax; 1:1,000; cat. no. BS6420), anti-cleaved caspase-3 (1:1,000; cat. no. BS7004), anti-Nrf2 (1:1,000; cat. no. BS1258), anti-glutamate cysteine ligase modifier (GCLM; 1:1,000; cat. no. BS2927), anti-Akt (1:1,000; cat. no. BS90043), anti-PI3K (1:1,000; cat. no. BS9852M), anti-p-PI3K (1:1,000; cat. no. AP0153), anti-ERK (1:1,000; cat. no. BS1968), anti-p-ERK (1:1,000; cat. no. BS4759), anti-glyceraldehyde 3-phosphate dehydrogenase (GAPDH; 1:1,000; cat. no. AP0063), anti-cytochrome *c* oxidase IV (COX IV; 1:600; cat. no. AP0705), anti-histone 3 (H3; 1:1,000; cat. no. BS1161), and anti-β-actin (1:1,000; cat. no. AP0060), all from Bioworld Technology, Inc.. Anti-HO-1 (1:1,000; cat. no. 66743-1), anti-NAD(P)H:quinone oxidoreductase 1 (NQO1; 1:1,000; cat. no. 11451-1-AP), from Proteintech Group, Inc.. Anti-phosphorylated (p)-Akt (1:1,000; cat. no. #4060s; Cell Signaling Technology, Inc.), anti-cytochrome *c* (cyt-c, 1:600; cat. no. AF2047; Beyotime Institute of Biotechnology). Following washing with PBS containing 0.05% (v/v) Tween-20 (PBST), the membranes were incubated with horseradish peroxidase-conjugated anti-mouse IgG (1:0000; cat. no. #7076; Cell Signaling Technology Inc.) or horseradish peroxidase-conjugated anti-rabbit IgG (1:0000; cat. no. SA00001-2; ProteinTech

Group, Inc.), and bands were visualized using Enhanced Chemiluminescence Reagent kit (Beyotime Institute of Biotechnology; cat. no. P0018S). Membranes were imaged using the iBright FL1000 Imaging System (Invitrogen; Thermo Fisher Scientific, Inc.). Image J software 1.53a (National Institutes of Health) was used to quantify the gray value of western blot bands and protein expression level was normalized as the gray value of the target protein/the loading control protein.

Reverse transcription-quantitative PCR (RT-qPCR). Total RNA was extracted using a Total RNA extraction kit (Tiangen Biotech Co., Ltd.) according to the manufacturer's instructions, and perform reverse transcribed according to Prime Script RT reagent kit instructions (Takara Biotechnology Co., Ltd.). Aliquots of cDNA were subjected to qPCR analysis with SYBR Green PCR Master Mix (Takara Biotechnology Co., Ltd.) and a Real-Time PCR system equipped with a CFX 96 Connect™ Optics Module (Bio-Rad Laboratories, Inc.). Reaction program [94˚C pre-denaturation for 30 sec; 40 cycles (94˚C denaturation for 5 sec, 60˚C annealing for 1 min)]. Primer sets specific to GAPDH (reference gene) and NRF2 were as follows: GAPDH forward, 5'-ACCACAGTCCATGCCATCAC-3' and reverse, 5'-TCCACCACCCTGTTGCTGTA-3'; NRF2 forward, 5'-CAG TCAGCGACGGAAAGAGT-3' and reverse, 5'-ACGTAGCCG AAGAAACCTCA-3'. Data were analyzed according to the $2^{-\Delta\Delta cq}$ method as previously described (18).

Drosophila stocks, husbandry, and lifespan analysis. Drosophila (including W^-, UAS-CncC, UAS-CncC RNAi and *da*-Gal4) were obtained from Dr Yufeng Yang (Institute of Life Sciences, Fuzhou University, Fuzhou, China). UAS-CncC RNAi x *da*-Gal4 was obtained by mating UAS-CncC RNAi and *da*-Gal4. Flies were grown on sugar-yeast-agar medium with or without Re (final concentration 0.4 mM in DMSO) and Rot (final concentration 515 μM in DMSO), which was replenished daily and the number of deaths of flies was recorded. Flies were incubated in a humidified (50% relative humidity), temperature-controlled (29˚C) incubator with a 12-h on/off light cycle. The significance of the survival curve was calculated using the Log-rank (Mantel-Cox) test.

Drosophila negative geotaxis (climbing) assay. On the day of the assay, flies were anesthetized with CO_2 and transferred into a glass pipette (height 22 cm, diameter 1.0 cm, capacity 25 ml) capped with a cotton plug. Following recovery, the flies were left for 15 min and the glass pipette was then placed vertically and flies were shaken down to the bottom of the tube. Data were recorded by taking photographs at 5 sec intervals for a total of 1 min. The climbing index was evaluated as follows. The fly movement area (18 cm from the bottom of the pipette to the lower end of the plug) was divided into 2-cm zones (1, 2, 3, 4, 5, 6, 7, 8, 9) from the bottom to the top. The climbing index was calculated as the total number of flies in each area multiplied by the number of regions.

Determination of hydrogen peroxide (HP) level in Drosophila. To evaluate the HP level in *Drosophila* a hydrogen peroxide detection kit (cat. no. BC3590; Beijing Solarbio Science & Technology Co., Ltd.) Weigh about 0.1 g flies tissue and add 1 ml working solution for ice bath homogenization; centrifuged 8,000 x g at 4˚C for 10 min, all supernatant was taken and placed on ice for testing. Add corresponding reagents according to the kit instructions, and use a microplate reader (Tecan Group, Ltd.) to detect at 415 nm.

ATP analysis, respirometry analysis and ROS production. ATP analysis and respiration measurement analysis methods were performed as previously described (19). Flies were homogenized in 500 μl PBS by a cell disruptor, centrifuged at 530 x g for 5 min at room temperature, and incubated in DCFH-DA (final concentration 20 μM; cat. no. CA1410; Beijing Solarbio Science & Technology Co., Ltd.) for 30 min at 37˚C. ROS was measured with an Infinite® 200 Pro microplate reader (Tecan Group, Ltd.) using excitation at 488 nm and emission at 530 nm (20).

Immunofluorescence microscopy of Drosophila. Flies were anesthetized by CO_2 and next fixed in 4% paraformaldehyde at 25˚C for 2.5 h, washed with PBST, and the brains were dissected and placed in blocking agent (PBS buffer; 0.1% Triton X-100; 10% heat-inactivated fetal bovine serum) at 25˚C for 90 min. The blocking agent was removed and replaced with anti-tyrosine hydroxylase (TH) antibody (1:500; cat. no. AB152; Millipore corporation) overnight at 4˚C in the dark. The brains were washed with pre-cooled PBST buffer, incubated with Rabbit anti-goat IgG antibody, FITC conjugate (1:200; cat. no. AP106F; Millipore corporation) for 2 h at 25˚C in the dark, and washed again. Finally, the brains were mounted onto slides and imaged immediately with a laser confocal microscope.

Statistical analysis. Data are expressed as the mean ± standard deviation (SD). Data were evaluated using GraphPad Prism 6.0 software (GraphPad Software, Inc.). All experiments in the present study were repeated three times. Group means were compared using one-way analysis of variance (ANOVA) test followed by Tukey's post hoc tests. $P \leq 0.05$ was considered to indicate a statistically significant difference.

Results

Re protects SH-SY5Y cells against the cytotoxic effects of Rot. Rot has been shown to reproduce numerous features of PD in animal models (21); therefore, its effects *in vitro* were examined using the human neuroblastoma cell line SH-SY5Y. The results revealed that Rot alone significantly decreased cell viability (Fig. S1). The antioxidant and neuroprotective effects of ginseng are mediated by ginsenosides, the main active components of ginseng (22). To assess these compounds, the optimal nontoxic concentrations of five representative ginsenosides: Rg1, Rg2, Rg3 and Rh2 (Fig. S2), as well as Re (Figs. 1A and B, and S3A) were first determined using the CCK-8 cell viability assay. The protective effect of each monomer saponin on Rot-treated SH-SY5Y cells was then examined (Figs. S4, 1C and S3B). Among the ginsenosides assessed, Re had the most significant protective effect on Rot-induced SH-SY5Y cytotoxicity (Figs. 1D and S3C; Table SI). Re was protective at 2.5, 5, and 10 μM, with maximal protection observed at 5 μM Re (Figs. 1C and S3B). Moreover, there was no significant difference between the protective effects

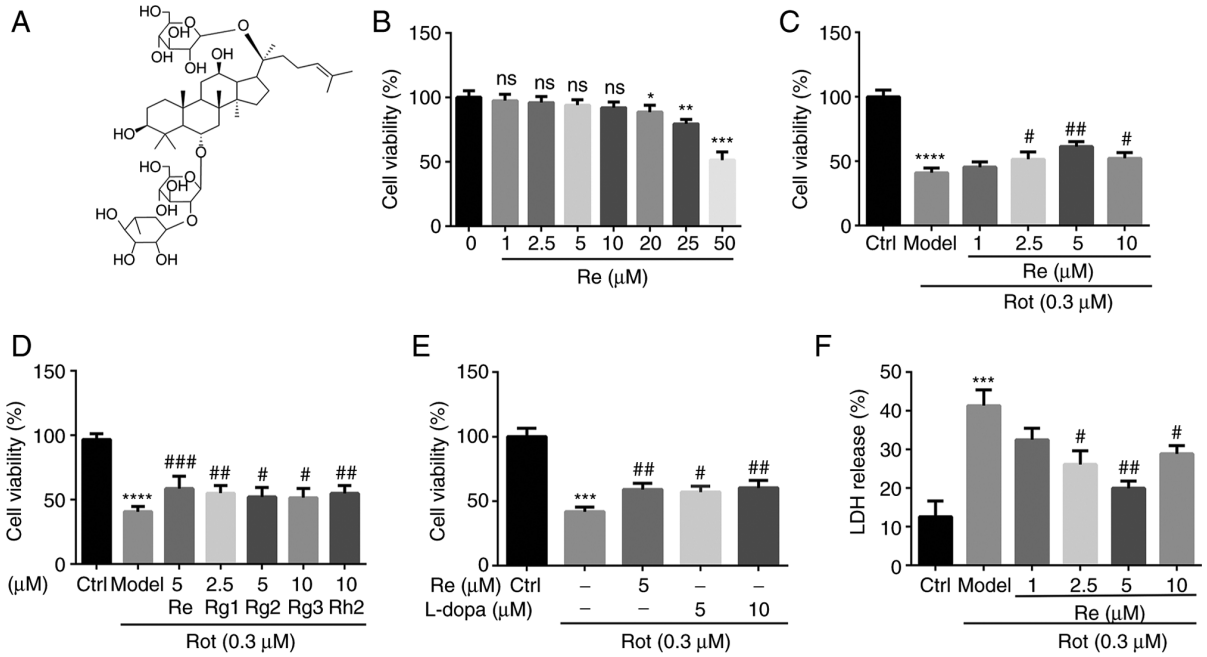

Figure 1. Re attenuates Rot-induced cytotoxicity in SH-SY5Y cells. (A) Chemical structure of Re. (B) Detection of Re cytotoxicity in SH-SY5Y cells assessed by CCK-8 assay. (C) Effect of Re on the viability of SH-SY5Y cells treated with Rot assessed by CCK-8 assay. (D) Comparison of the effects of ginsenoside monomers (Re, Rg1, Rg2, Rg3, and Rh2; purity ≥98%) on the viability of SH-SY5Y cells treated with Rot. (E) Analysis of the effects of Re and l-dopamine on the viability of SH-SY5Y cells treated with Rot. The above experiments calculated the relative cell viability using an endpoint time of 24 h. (F) LDH release cytotoxicity assay. Data are expressed as the mean ± SD; n=3. *P<0.05, **P<0.01, ***P<0.001 and ****P<0.0001 vs. the control; $^{\#}$P<0.05, $^{\#\#}$P<0.01 and $^{\#\#\#}$P<0.001 vs. Rot treatment alone. Re, ginsenoside Re; Rot, rotenone; CCK-8, Cell Counting Kit-8; l-dopa, l-dopamine; LDH, lactate dehydrogenase.

of Re at 5 μM and l-dopa at 5 or 10 μM (Figs. 1E and S3D). Re also displayed significant protection when Rot-induced cytotoxicity was measured using a LDH release assay (Fig. 1F).

Re attenuates Rot-induced apoptosis of SH-SY5Y cells. To determine whether Rot-induced cell death was mediated by triggering of apoptosis, the cells were stained with Annexin V-FITC and propidium iodide (PI) and analyzed by flow cytometry. The results showed that exposure to Rot (0.3 μM) alone increased the abundance of cells in early [Annexin V-FITC^{+}, PI^{-} (R4)] and late [Annexin V-FITC^{+}, PI^{+} (R5)] apoptosis (total up to 33.97%), and that Re co-treatment significantly reduced the apoptotic rate (Fig. 2A and B). Similarly, microscopic analysis showed that SH-SY5Y cells treated with Rot exhibited the typical morphological characteristics of apoptosis, whereas Re co-treated cells exhibited a lower level of Hoechst 33342 staining and had uniformly stained chromatin, comparable to the untreated control cells (Fig. 2C). Cell apoptosis is regulated in part by a balance between the expression of the anti-apoptotic and pro-apoptotic regulatory proteins Bcl-2 and Bax (23). Therefore, the expression of these proteins in Rot and Re co-treated cells was examined by western blot analysis. Notably, the ratio of Bax to Bcl-2 protein was increased by Rot treatment and decreased by co-incubation of Rot-treated cells with Re (Fig. 2D).

Re reduces Rot-induced mitochondrial dysfunction and suppresses activation of the mitochondrial apoptotic pathway in SH-SY5Y cells. Mitochondrial function was assessed in SH-SY5Y cells following Rot and/or Re treatment using several methods. First, the cells were labeled with JC-1, an MMP probe. In healthy cells, green-fluorescent JC-1 monomers accumulate in mitochondria and form red-fluorescent aggregates. Loss of MMP results in formation of JC-1 monomers; thus, the ratio of green/red fluorescence is a marker of MMP integrity and reflects mitochondrial health (24). Rot-treated cells exhibited an increase in green fluorescence compared with the red JC1 aggregates in control cells, which was reduced by co-treatment with Re (Fig. 3A). As a second method of MMP analysis, the cells were labeled with the fluorescent dye rhodamine 123. In healthy cells, rhodamine 123 selectively enters the mitochondrial matrix and emits bright yellow-green fluorescence; however, cells undergoing apoptosis or necrosis experience disruption of the MMP, which leads to opening of the mitochondrial permeability transition pore, release of rhodamine 123 from the mitochondria, and a reduction in mitochondrial fluorescence (25). Notably, the results obtained when MMP was assessed by rhodamine 123 labeling (Fig. 3B) were similar to those obtained using the JC-1 labeling method. Finally, ATP generation, as a third indicator of mitochondrial health in SH-SY5Y cells, was also detected. As expected, Rot-treated cells contained less ATP than the control cells, and Re significantly reversed these deleterious effects of Rot (Fig. 3C).

To determine whether the observed increase in SH-SY5Y cell apoptosis induced by Rot (Fig. 2) was mediated by the exogenous receptor-activated pathway or the endogenous mitochondrial pathway, the release of the mitochondrial enzyme cyt-c into the cytosol, a key feature of endogenous apoptosis (26), was examined, as well as the activity of caspases, which are the main effector enzymes of apoptosis (27). As expected, Rot treatment increased cyt-c release and stimulated the activities of caspase-3, -8, and -9; however, co-treatment with Re attenuated the effects of Rot on each of these parameters except activation

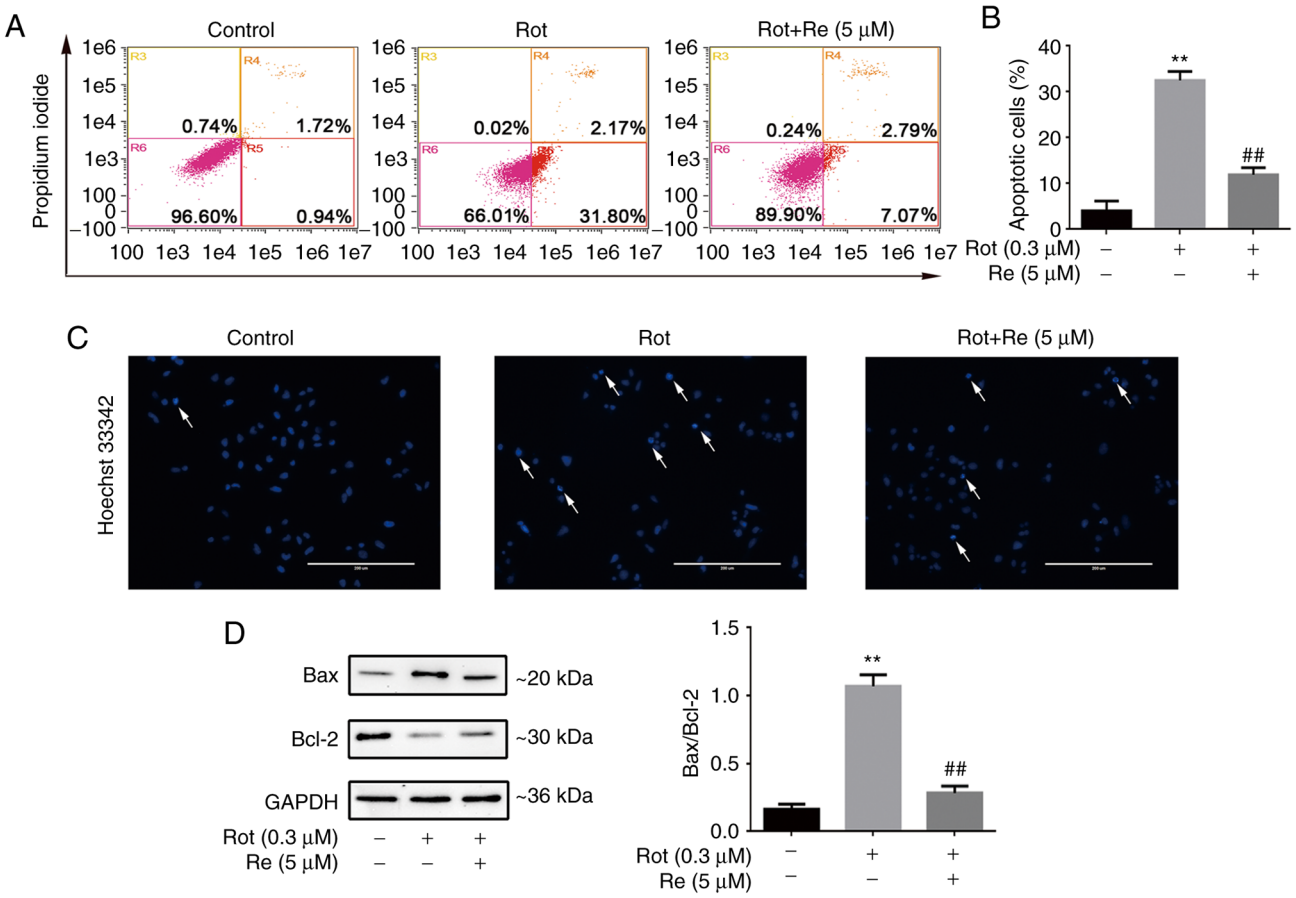

Figure 2. Re reduces Rot-induced apoptosis in SH-SY5Y cells. (A) Apoptotic cells assessed by Annexin V-FITC/propidium iodide staining and flow cytometry. (B) Quantification of apoptosis determined in A. (C) Nuclear morphology of apoptosis-associated changes in Hoechst 33342-stained cells. Scale bar, 200 μm. White arrows represent nuclei with intense fluorescence and an irregular shape. (D) Western blot analysis of Bax and Bcl-2 expression. Data are expressed as the mean ± SD; n=3. **P<0.01 vs. the control; $^{\#\#}$P<0.01 vs. Rot treatment alone. Re, ginsenoside Re; Rot, rotenone; Bax, Bcl-2 associated X protein; B-cell lymphoma-2.

of caspase-8 (Fig. 3D-F). Collectively, these results suggest that Re-mediated protection against Rot-induced cell injury involves attenuation of mitochondrial dysfunction and inhibition of the mitochondrial apoptotic pathway.

Re reduces Rot-induced oxidative stress in SH-SY5Y cells. To determine whether Re affects Rot-induced oxidative stress in SH-SY5Y cells, several metabolites that undergo characteristic changes in expression upon cell exposure to oxidative stress were assessed. These included ROS, the fatty acid oxidation product, MDA, and the antioxidants GSH-Px, an enzyme that catalyzes reduction of lipid peroxides by GSH, and SOD, which catalyzes the dismutation of superoxide anions and is an important antioxidant enzyme (28). Rot treatment alone resulted in increased levels of ROS and MDA, decreased levels of GSH, and reduced SOD and GSH-Px activities (Fig. 4). Notably, each of these Rot-induced effects was reversed in cells co-treated with Re (Fig. 4), demonstrating that Re is able to counteract Rot-induced oxidative stress.

Re reduces Rot-induced oxidative stress via effects on the antioxidant transcription factor Nrf2 in SH-SY5Y cells. Nrf2 is a key component of the oxidative stress response and regulates the expression of antioxidant and cytoprotective genes (29). To determine whether Nrf2 is modulated by Rot and/or Re treatment, western blot analysis of SH-SY5Y subcellular fractions was performed. Compared with the untreated control cells, Rot treatment induced no significant change in the distribution of Nrf2 in the cytoplasm and nucleus, whereas Re-co-treated cells showed an increase in nuclear localization of Nrf2 (Fig. 5A). Nrf2 is generally cytosolic but translocates to the nucleus in response to oxidative stress, where it binds to antioxidant response elements and induces transcription of genes such as HO-1, GCLM, NQO1 (30). Consistent with this, Re treatment also significantly increased the expression of HO-1, GCLM, and NQO1 proteins (Fig. 5B).

To determine the importance of Nrf2 in Re-mediated protection against Rot, the cells were transfected with a control siRNA or Nrf2-targeting siRNA (Fig. 5C). The beneficial effects of Re on Rot-induced cytotoxicity (Fig. 5D) and ROS production (Fig. 5E and F) were reduced in siNrf2-transfected cells compared with control cells. Collectively, these results indicated that Nrf2 plays an essential role in Re-mediated neuroprotection against oxidative stress.

Re induces Nrf2 nuclear transport via the PI3K/AKT and ERK signaling pathways in SH-SY5Y cells. To determine which signaling pathways mediate Re-induced Nrf2 activation, SH-SY5Y cells were pretreated with inhibitors of PI3K/AKT (LY294002, 15 μM), JNK (SP600125, 10 μM),

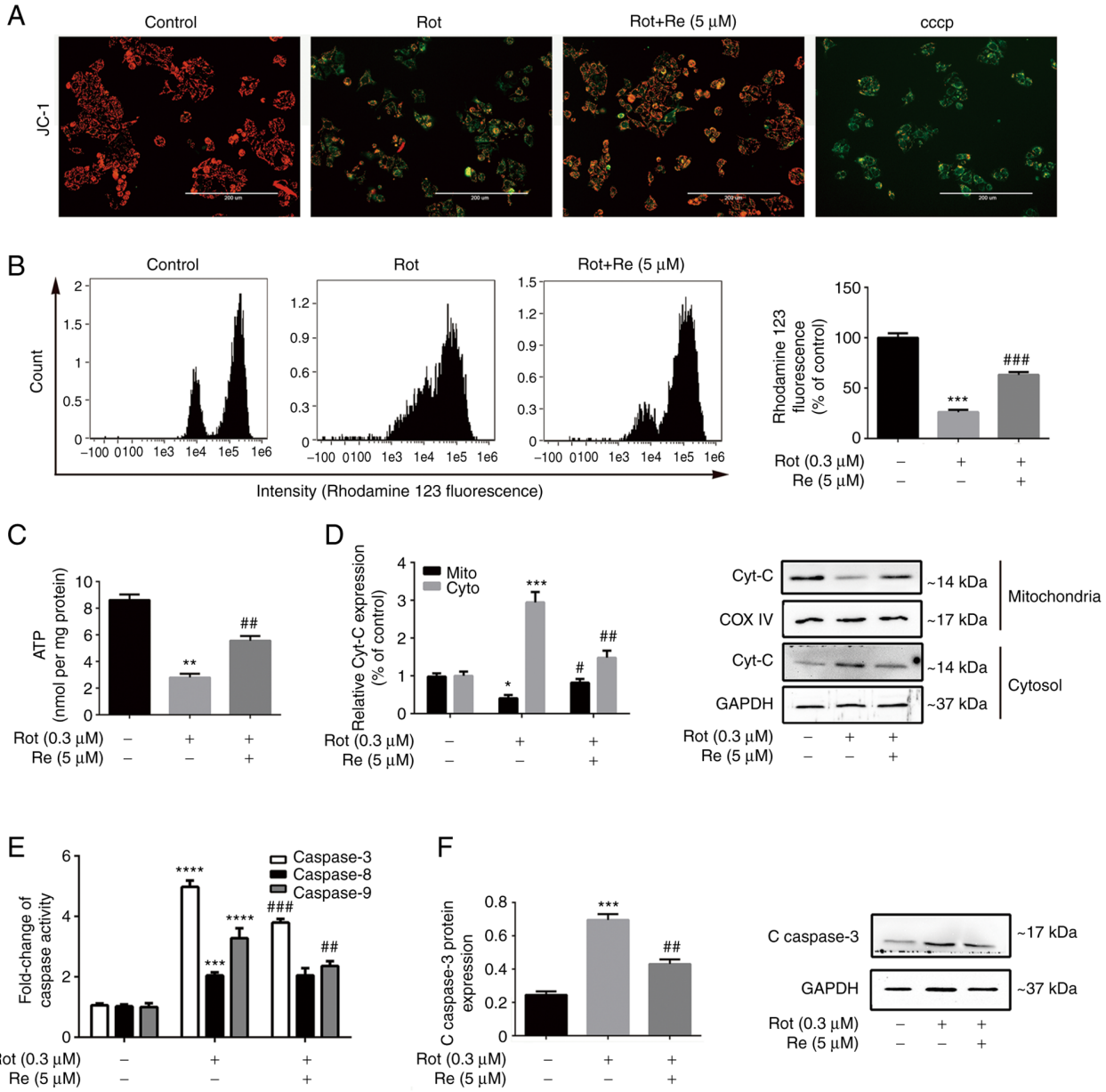

Figure 3. Re alleviates Rot-induced mitochondrial dysfunction in SH-SY5Y cells. (A) Fluorescence microscopic images of JC-1-stained cells to assess the MMP. Scale bar, 200 μm. (B) Flow cytometric analysis of loss of MMP integrity. (C) Quantification of ATP production. (D) Western blot analysis of cytochrome *c* subcellular localization. (E) Quantification of caspase-3, caspase-8, and caspase-9 activities. (F) Western blot analysis of cleaved caspase-3 expression. Data are expressed as the mean ± SD; n=3. *P<0.05, **P<0.01, ***P<0.001 and ****P<0.0001 vs. the control; $^{\#}$P<0.05, $^{\#\#}$P<0.01 and $^{\#\#\#}$P<0.001 vs. Rot treatment alone. Re, ginsenoside Re; Rot, rotenone; MMP, mitochondrial membrane potential; ATP, adenosine triphosphate; Cyt-c, cytochrome *c*; COX IV, cytochrome *c* oxidase IV.

ERK (PD98059, 15 μM), AMPK (CC, 10 μM), and p38 MAPK (SB203580, 5 μM) and then the effects on Re activity were analyzed in cell viability assays. Compared with cells incubated under control conditions, LY294002 and PD98059 treatment significantly suppressed the protective effect of Re on Rot-induced cell viability (Fig. 6A) and ROS production (Fig. 6B; P<0.05), whereas the remaining inhibitors had no effect. The ERK and PI3K/AKT inhibitors prevented Re-stimulated nuclear localization of Nrf2 in SH-SY5Y cells (Fig. 6C). In addition, ROS levels, Nrf2 expression in the nucleus, and cell viability were all significantly altered by cell treatment with AKT inhibitor IV (Fig. S5). Confirming these associations, it was determined that Rot downregulated the expression of p-AKT (Fig. 6D and E), p-ERK (Fig. 6D and F) and phosphorylated (activated) PI3K (Fig. 6D and G), and these effects were significantly reversed by treatment with Re.

Re attenuates Rot-induced locomotor defects and neuron loss in Drosophila. Exposure of *Drosophila* to Rot mimics numerous of the features of human PD and is widely used as a model for investigating the pathogenesis of PD (31). Consistent with the aforementioned study, it was determined that exposure of flies to 515 μM Rot for 7 days before analysis caused a loss of dopaminergic neurons, as measured by staining of *Drosophila* brains for the marker protein TH

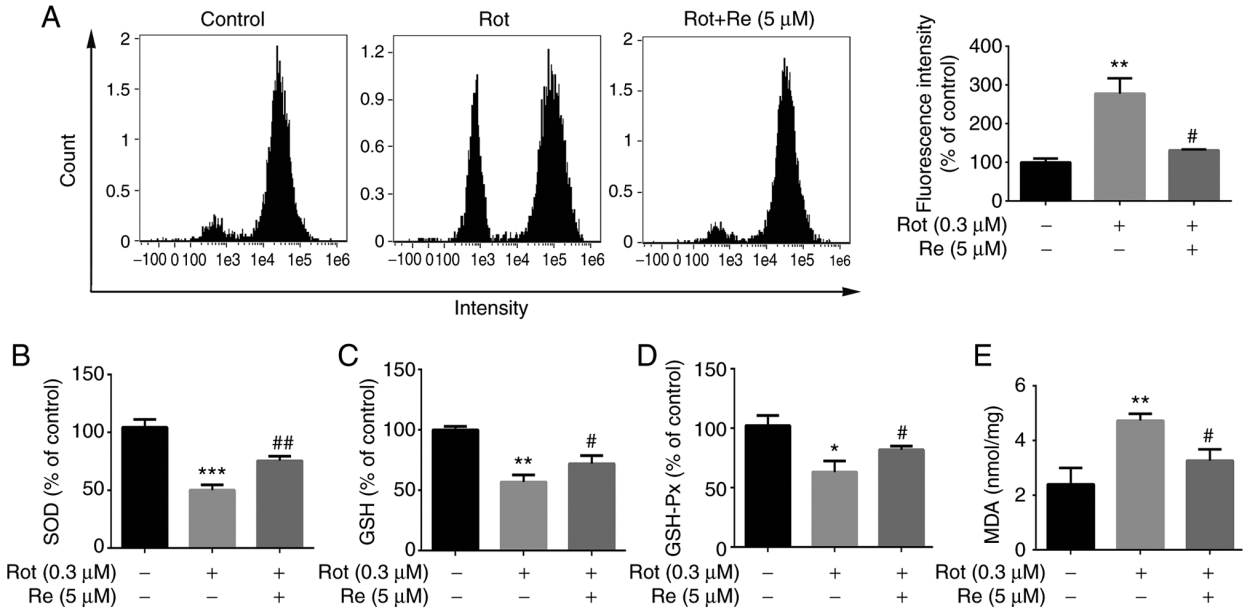

Figure 4. Re reduces Rot-induced oxidative stress in SH-SY5Y cells. Measurement of intracellular (A) ROS levels, (B) SOD activity, (C) GSH concentration, (D) GSH-Px activity and (E) MDA concentration. Data are expressed as the mean ± SD; n=3. *P<0.05, **P<0.01 and ***P<0.001 vs. the control; $^{\#}$P<0.05 and $^{\#\#}$P<0.01 vs. Rot treatment alone. Re, ginsenoside Re; Rot, rotenone; ROS, reactive oxygen species; SOD, superoxide dismutase; GSH, glutathione; GSH-Px, glutathione peroxidase; MDA, malondialdehyde.

(Fig. 7A and B). However, flies that had been administered Rot plus Re (0.4 mM) showed partial reversal of neuron loss (Fig. 7C). Since Rot-induced dopaminergic neurotoxicity has been reported to cause locomotor deficits (32), the effects of Re treatment on fly movement were also examined. Exposure of flies to 515 μM Rot reduced their climbing ability to 39.3% compared with control flies, as measured by a quantitative climbing index (Fig. 7D). However, co-treatment of flies with Re (0.4 mM) significantly reversed the effect of Rot and increased the climbing index to 61.3% of that observed for the control flies (Fig. 7D).

Re rescues Rot-induced oxidative damage and mitochondrial dysfunction in Drosophila. Finally, whether reversal of Rot-induced oxidative stress and mitochondrial dysfunction contribute to the protective effects of Re were determined in the *Drosophila* PD model. Mitochondria are the predominant site of ATP production in cells, and changes in cellular ATP content can indicate impaired mitochondrial function (33). Accordingly, a reduction in ATP levels in Rot-treated flies was observed that was reversed by Re co-treatment (Fig. 8A). Consistent with a previous study, mitochondrial respiratory chain complex I (NADH oxidase) has been demonstrated to be related to the occurrence of PD (34). However, mitochondrial respiratory chain complex II (succinate dehydrogenase), which is the main element of electrons entering the mitochondrial electron transport chain (35), also exhibited a positive effect of Re in flies (Fig. 8B and C). Re also reduced the Rot-induced increase in ROS (Fig. 8D) and HP (Fig. 8E). However, Re had no significant effect on the survival curve of Rot-treated flies (UAS-CncC RNAi x *da*-Gal4) (Fig. 8F). Overall, these results indicated that the neuroprotective effect of Re in the *Drosophila* PD model was consistent with that detected using the SH-SY5Y cell model *in vitro*.

Discussion

Re was previously shown to have neuroprotective properties in several models of neurological diseases, including PD. In the 1-methyl-4-phenyl-1,2,3,6-tetrahydropyridine mouse model of PD, Re protected nigral neurons from apoptosis, reduced carbon tetrachloride-induced cell loss and degeneration, and maintained TH^{+} cell and neurite numbers (32). Re had previously been shown to cross the blood-brain barrier in adult rats (36), further demonstrating that Re has a better application prospect in neuroprotection and PD treatment or prevention. In the present study, the protective effects of Re and other ginsenosides against Rot-induced toxicity were analyzed in a human neuroblastoma cell line and a *Drosophila* functional PD model. The ginsenosides assessed were selected because they have been reported to be protective in PD models *in vivo* or *in vitro (*37). At optimal concentrations, Re had the most potent effects among the compounds examined. Notably, no significant differences between the cytoprotective effects of Re and l-dopa were observed. The neuroprotective effects of Re *in vitro* were also observed in the *in vivo Drosophila* model, in which Re co-treatment reduced Rot-induced loss of TH^{+} neurons and partially restored the defects in motor behavior. Thus, the results of the present study further confirm previous suggestions that Re may be the main active ingredient in ginseng and its effects on PD.

Multiple studies have described the neuroprotective effect of ginsenosides such as Re, including their ability to inhibit apoptosis (38-40). The results of the present study confirmed this in SH-SY5Y cells, and additionally demonstrated that Re reduces the characteristic changes in morphology associated with apoptosis. Two major apoptotic pathways have been described. In the exogenous pathway, apoptosis is triggered by extracellular signals that initiate a cascade of events leading to

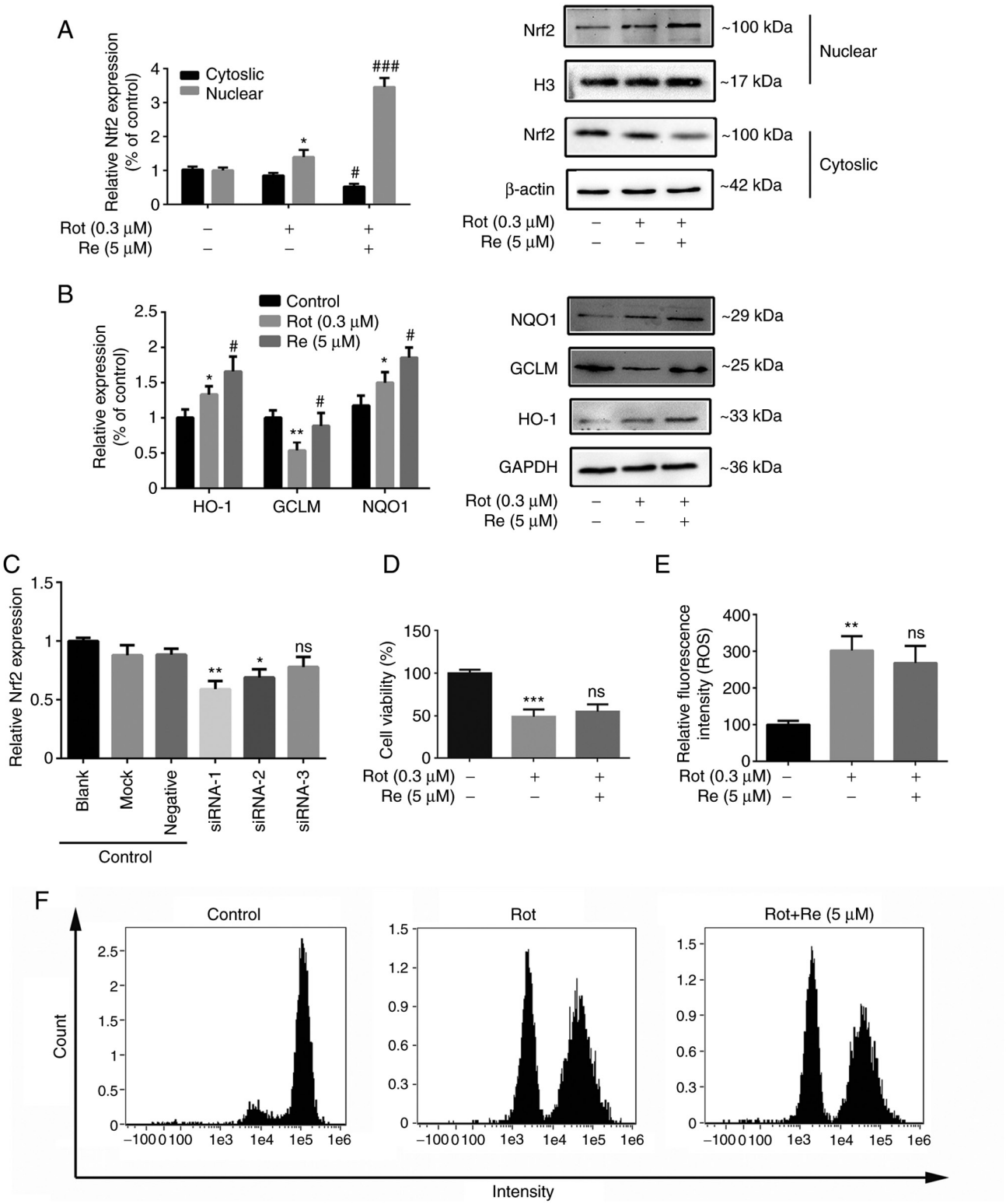

Figure 5. Re reduces Rot-induced cytotoxicity and ROS accumulation via Nrf2. (A and B) Western blot analysis of the expression of (A) Nrf2 and (B) HO-1, GCLM and NQO1. (C) Silencing of Nrf2 expression by transfection with gene-specific siRNA. Knockdown efficiencies were 41% for siRNA-1, 31% for siRNA-2, and 22% for siRNA-3. Further cell viability and ROS level determinations were performed using the most efficient siRNA, siRNA-1. (D) CCK-8 assay of cell viability after transfection of SH-SY5Y cells with Nrf2 siRNA-1. (E) The intracellular ROS quantification and (F) flow cytometric plots of Nrf2 siRNA-1 transfected cells. Data are expressed as the mean ± SD; n=3. *P<0.05, **P<0.01 and ***P<0.001 vs. the control; $^{\#}$P<0.05 and $^{\#\#\#}$P<0.001 vs. Rot treatment alone. Re, ginsenoside Re; Rot, rotenone; ROS, reactive oxygen species; Nrf2, nuclear factor erythroid 2-related factor 2; HO-1, heme oxygenase-1; GCLM, glutamate cysteine ligase modifier; NQO1, NAD(P)H:quinone oxidoreductase 1; siRNA, small interfering RNA; CCK-8, Cell Counting Kit-8.

caspase-8 activation; in the endogenous pathway, mitochondria release factors that lead to activation of caspases-3 and -9 (41). In the present study it was demonstrated that Rot induced loss of MMP integrity, cyt-c release into the cytoplasm, activation of caspases-3 and -9, and additionally decreased the ratio of the pro-/anti-apoptotic proteins Bax/Bcl-2. Re inhibited these

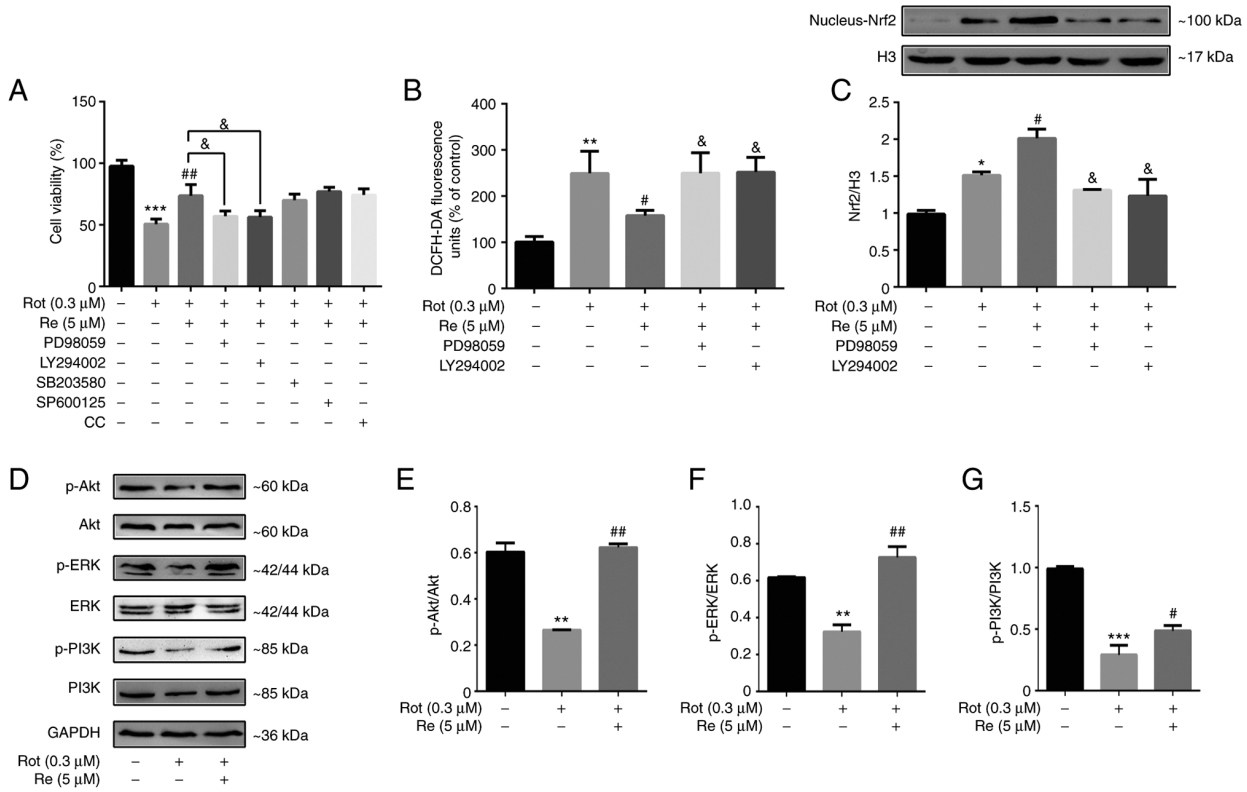

Figure 6. Re-induced Nrf2 accumulation is mediated by PI3K/AKT and ERK. (A) Cell viability assessed by CCK-8 assay. (B) Quantification of ROS levels assessed by the DCFH-DA assay and detected by fluorescence microplate reader. The excitation wavelength was 488 nm, and the emission wavelength was 530 nm. (C) Western blot analysis of nuclear Nrf2 protein levels. Cells were pretreated with 15 μM PD98059 (ERK1/2 inhibitor), 15 μM LY294002 (PI3K/AKT inhibitor), 5 μM SB203580 (p38 MAPK inhibitor), 10 μM SP600125 (JNK inhibitor), or 10 μM CC (AMPK inhibitor) for 1 h and then treated with 0.3 μM Rot and 5 μM Re for 24 h. (D) Representative western blot images of PI3K/AKT and ERK pathways. Semi-quantitative analysis of (E) p-Akt, (F) p-ERK and (G) p-PI3K protein expression in SH-SY5Y cells. Data are presented as the mean ± SD; n=3. *P<0.05, **P<0.01 and ***P<0.001 vs. the control; $^{\#}$P<0.05 and $^{\#\#}$P<0.01 vs. Rot treatment alone; $^{\&}$P<0.05 vs. Re+Rot treatment. Re, ginsenoside Re; Nrf2, nuclear factor erythroid 2-related factor 2; PI3K, phosphatidylinositol 3-kinase; AKT, protein kinase B; ERK, extracellular regulated protein kinase; CCK-8, Cell Counting Kit-8; DCFH-DA, 2,7-dichlorofluorescein diacetate; MAPK, p38 mitogen-activated protein kinase; JNK, Jun N-terminal kinase; CC, Compound C; AMPK, adenosine 5'-monophosphate (AMP)-activated protein kinase; Rot, rotenone; p-, phosphorylated.

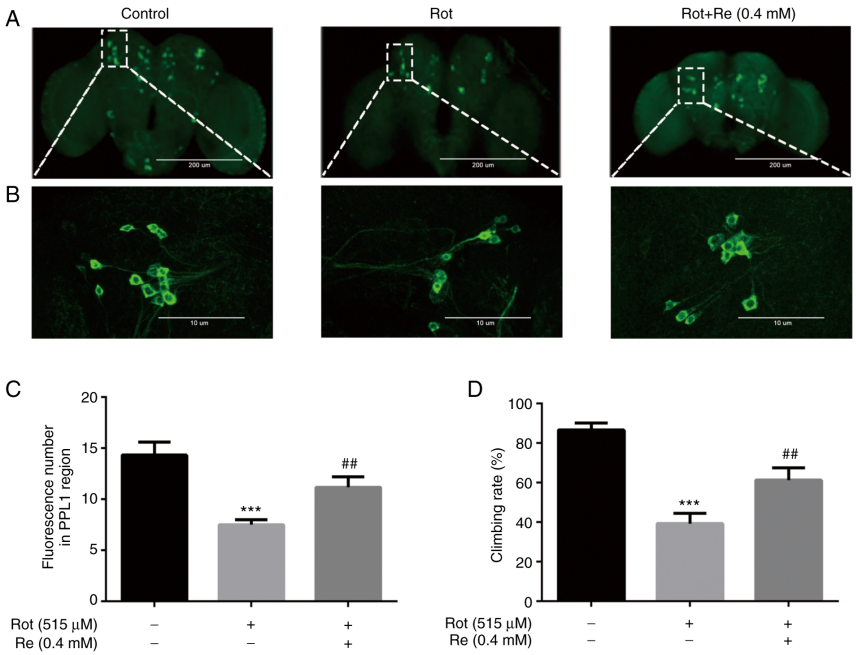

Figure 7. Effect of Re on locomotor deficiency and dopaminergic neuron loss in Rot-treated *Drosophila*. (A) Immunostaining of TH^{+} dopaminergic neurons in the brains of *Drosophila* (n=8 flies per condition). Scale bar, 200 μm. (B) Locally enlarged clusters of dopaminergic neurons in the PPL1 region of the brain of the fly. Scale bar, 10 μm. (C) Columnar statistical analysis of the distribution of TH in the PPL1 region of the brain of the fly. (D) Columnar statistical analysis of the climbing index of flies treated with 515 μM Rot with or without 0.4 mM Re (n=50 flies per condition). ***P<0.001 vs. the control; $^{\#\#}$P<0.01 vs. Rot treatment alone. Re, ginsenoside Re; Rot, rotenone; TH, tyrosine hydroxylase; PPL1, protocerebral posterior lateral 1.

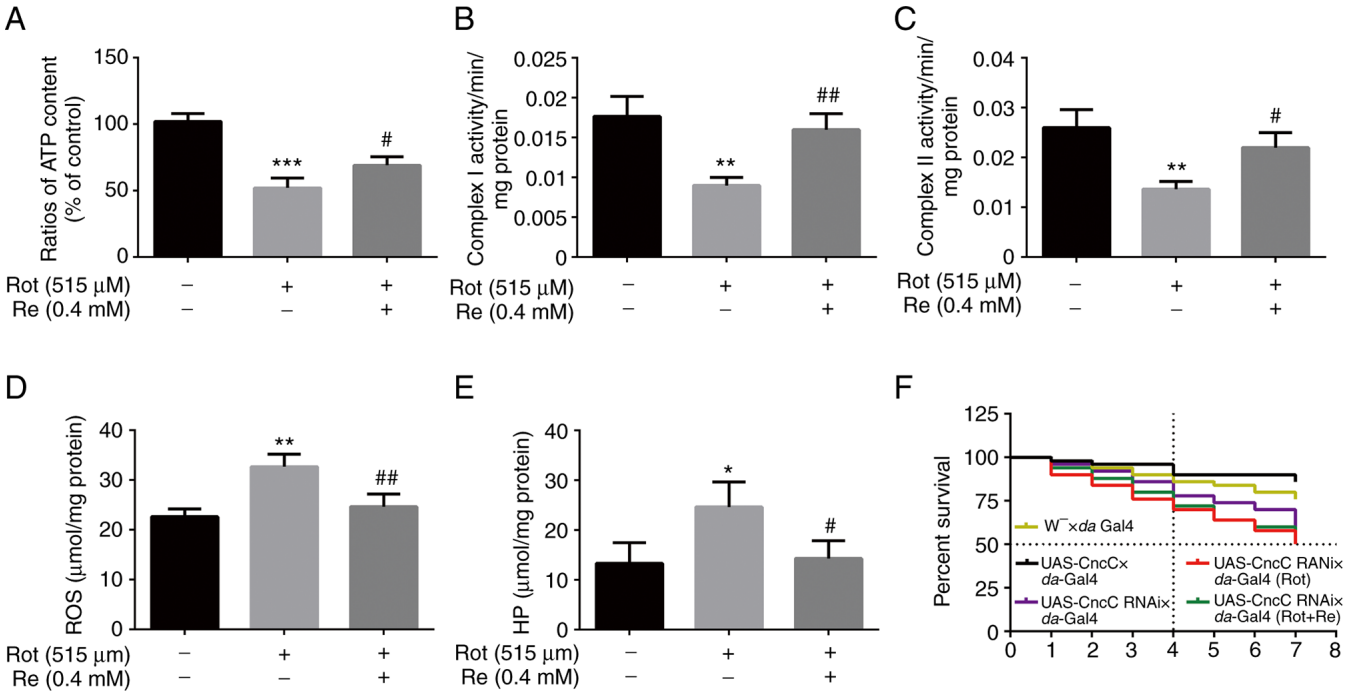

Figure 8. Re rescues Rot-induced oxidative stress and mitochondrial dysfunction in *Drosophila*. Flies were treated with 515 μM Rot with or without 0.4 mM Re and analyzed for (A) ATP levels, (B) mitochondrial respiratory chain complex I levels, (C) mitochondrial respiratory chain complex II levels, (D) ROS levels, and (E) HP levels. (F) Life survival curve of *Drosophila*; n=50 flies per condition. *P<0.05, **P<0.01 and ***P<0.001 vs. the control; $^{\#}$P<0.05 and $^{\#\#}$P<0.01 vs. Rot treatment alone. Re, ginsenoside Re; Rot, rotenone; ATP, adenosine triphosphate; ROS, reactive oxygen species; HP, hydrogen peroxide.

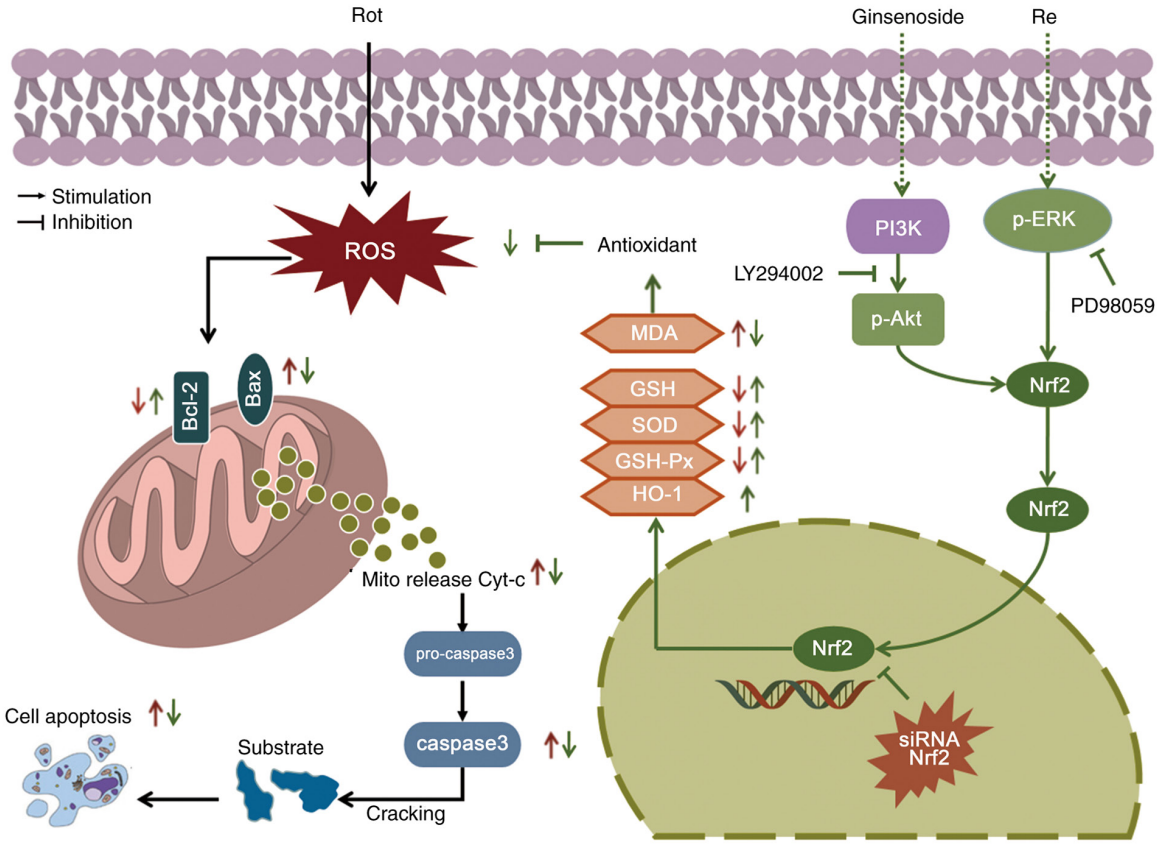

Figure 9. Scheme summarizing the neuroprotective effects of Re. *In vitro* and *in vivo* experimental models of PD showed that treatment with Re prevents apoptosis induced by Rot-stimulated oxidative stress and mitochondrial dysfunction via a mechanism involving the PI3K/AKT, ERK, and Nrf2/HO-1 pathways. Re, ginsenoside Re; PD, Parkinson's disease; Rot, rotenone; PI3K, phosphatidylinositol 3-kinase; AKT, protein kinase B; ERK, extracellular regulated protein kinase; Nrf2, nuclear factor erythroid 2-related factor 2; HO-1, heme oxygenase-1; ROS, reactive oxygen species; p-, phosphorylated; MDA, malondialdehyde; GSH, glutathione; SOD, superoxide dismutase; GSH-Px, glutathione peroxidase; GCLM, glutamate cysteine ligase modifier; NQO1, NAD(P)H:quinone oxidoreductase 1; siRNA, small interfering RNA; Cyt-c, cytochrome *c*; Bax, Bcl-2 associated X protein; B-cell lymphoma-2; siRNA, small interfering RNA.

apoptosis-related events, including the activation of caspase-3 and -9, but had no significant effect on caspase-8 activity. These results suggest that Re inhibits activation of the endogenous mitochondrial apoptotic pathway in this PD model and raises the possibility that this pathway could be a therapeutic target for PD. Notably, the protective effect of Re on mitochondrial function was also observed in the *Drosophila* PD model.

Oxidative stress is one of the main causes of human PD and Rot-mediated damage in animal PD models (42). A previous study by the authors demonstrated that Re prevents ROS generation in Aβ-induced SH-SY5Y cells (17), and findings in the present study revealed that Re suppressed Rot-triggered ROS production, which was consistent with that observation. GSH-Px, SOD, and GSH are important cellular antioxidants and have been widely studied due to their ability to remove oxygen free radicals *in vivo*. MDA content in cells indirectly reflects the lipid peroxidation rate and thus the degree of oxidative stress damage (43). The results of the present study suggest that Re strengthens the cellular antioxidant response by increasing SOD, GSH-Px, and GSH expression and reducing MDA content. Re also significantly improved Rot-induced compromise of the antioxidant capacity in the PD model in flies. These data clearly established that Re suppresses Rot-induced oxidative stress.

The Nrf2 activation pathway plays an important role in regulating the cellular response to oxidative stress, mainly by regulating the expression of antioxidant, anti-inflammatory, and detoxifying proteins (44). Modulation of this pathway therefore represents a potential target to prevent and treat PD. Re promotes the transport of Nrf2 into the nucleus and consequently increases the expression of oxidative stress response genes such as HO-1. Increased expression of HO-1 has been shown to protect against Rot-induced neurotoxicity (45). In the present study, it was determined that Rot modestly increased the nuclear transport of Nrf2 but the addition of Re to Rot-treated cells significantly increased Nrf2 nuclear localization and upregulated expression of HO-1. Moreover, siRNA-mediated Nrf2 silencing confirmed that Nrf2 activation is an essential component of the antioxidant and anti-apoptotic effects of Re. It was also observed that Re promoted phosphorylation of PI3K/AKT and ERK and that PI3K/AKT and ERK inhibitors significantly diminished the ability of Re to suppress apoptosis and ROS production in Rot-treated cells. Based on these results, it is theorized that Re may regulate Nrf2 activation and HO-1 expression via activation of the PI3K/AKT and ERK signaling pathways.

In summary, the key findings in the present study include: i) Re alleviates Rot-induced dopaminergic neuron loss and locomotor deficits in *Drosophila* and protects SH-SY5Y cells against Rot-induced apoptotic death *in vitro*; ii) inhibition of Rot-induced oxidative stress and increased expression of antioxidant enzymes are likely to be the dominant mechanisms by which Re exerts its neuroprotective effects; iii) the Nrf2 activation pathway contributes to Re-mediated neuroprotection against Rot; and iv) Re-induced Nrf2 activation may be mediated, at least in part, via activation of PI3K/AKT and ERK dual pathways (Fig. 9). In future, RNA-seq technology may be further used to comprehensively explore other potential signaling pathways of Re to delay the progression of PD.

Acknowledgements

The authors would like thank Dr Yufeng Yang from the Institute of Life Sciences, Fuzhou University, Fuzhou, China for providing us with the *Drosophila* for the experiment.

Funding

The present study was supported by the Key Project at Central Government Level: The Ability of Establishment of Sustainable Use for Valuable Chinese Medicine Resources (grant no. 2060302). In addition, it was also supported by the Science and Technology Project of Jilin Provincial Education Department (grant nos. JJKH20210966KJ and JJKH20210967KJ).

Availability of date and materials

The datasets used and/or analyzed during the current study are available from the corresponding author on reasonable request.

Authors' contributions

JQ, SL and ML conceived and designed the experiments. YL, SZ and WZ analyzed the data, prepared the figures, and helped with the writing of the manuscript. JQ and YZ performed the experiments and wrote the manuscript. SL and ML provided technical expertise and edited the article. JQ and ML confirm the authenticity of all the raw data. All authors read and approved the final manuscript, and agree to be accountable for all aspects of the research in ensuring that the accuracy or integrity of any part of the work are appropriately investigated and resolved.

Ethics approval and consent to participate

Not applicable.

Patient consent for publication

Not applicable.

Competing interests

The authors declare that they have no competing interests.

References

1. Zhang Y, Ren R, Sanford LD, Yang L, Zhou J, Tan L, Li T, Zhang J, Wing YK, Shi J, *et al*: Sleep in Parkinson's disease: A systematic review and meta-analysis of polysomnographic findings. Sleep Med Rev 51: 101281, 2020.
2. Ou Z, Pan J, Tang S, Duan D, Yu D, Nong H and Wang Z: Global trends in the incidence, prevalence, and years lived with disability of parkinson's disease in 204 countries/territories from 1990 to 2019. Front Public Health 9: 776847, 2021.
3. Choong CJ and Mochizuki H: Neuropathology of α-synuclein in Parkinson's disease. Neuropathology 42: 93-103, 2022.
4. Kurihara K, Mishima T, Fujioka S and Tsuboi Y: Efficacy and safety evaluation of safinamide as an add-on treatment to levodopa for parkinson's disease. Expert Opin Drug Saf 21: 137-147, 2022.
5. Uzuegbunam BC, Librizzi D and Hooshyar Yousefi B: PET radiopharmaceuticals for alzheimer's disease and parkinson's disease diagnosis, the current and future landscape. Molecules 25: 977, 2020.

6. Tabassum R and Jeong NY: Potential for therapeutic use of hydrogen sulfide in oxidative stress-induced neurodegenerative diseases. Int J Med Sci 16: 1386-1396, 2019.
7. Wilkaniec A, Cieślik M, Murawska E, Babiec L, Gąssowska-Dobrowolska M, Pałasz E, Jęśko H and Adamczyk A: P2X7 receptor is involved in mitochondrial dysfunction induced by extracellular alpha synuclein in neuroblastoma SH-SY5Y cells. Int J Mol Sci 21: 3959, 2020.
8. Feng ST, Wang ZZ, Yuan YH, Sun HM, Chen NH and Zhang Y: Update on the association between alpha-synuclein and tau with mitochondrial dysfunction: Implications for parkinson's disease. Eur J Neurosci 53: 2946-2959, 2021.
9. Lin KJ, Lin KL, Chen SD, Liou CW, Chuang YC, Lin HY and Lin TK: The overcrowded crossroads: Mitochondria, Alpha-Synuclein, and the Endo-Lysosomal system interaction in parkinson's disease. Int J Mol Sci 20: 5312, 2019.
10. Minato T, Nakamura N, Saiki T, Miyabe M, Ito M, Matsubara T and Naruse K: β-Aminoisobutyric acid, L-BAIBA, protects PC12 cells from hydrogen peroxide-induced oxidative stress and apoptosis via activation of the AMPK and PI3K/Akt pathway. IBRO Neurosci Rep 12: 65-72, 2021.
11. Li C, Tang B, Feng Y, Tang F, Pui-Man Hoi M, Su Z and Ming-Yuen Lee S: Pinostrobin exerts neuroprotective actions in neurotoxin-induced parkinson's disease models through Nrf2 induction. J Agric Food Chem 66: 8307-8318, 2018.
12. Brasil F, de Almeida F, Luckachaki M, Dall'Oglio E and de Oliveira M: The C-glucosyl flavone isoorientin pretreatment attenuates the methylglyoxal-induced mitochondrial dysfunction in the human neuroblastoma SH-SY5Y cells: Role for the AMPK-PI3K/Akt/Nrf2/γ-GCL/GSH axis. Metab Brain Dis: Mar 22, 2022 (Epub ahead of print).
13. Chiang NN, Lin TH, Teng YS, Sun YC, Chang KH, Lin CY, Hsieh-Li HM, Su MT, Chen CM and Lee-Chen GJ: Flavones 7,8-DHF, quercetin, and apigenin against tau toxicity via activation of TRKB signaling in ΔK280 TauRD-DsRed SH-SY5Y Cells. Front Aging Neurosci 13: 758895, 2021.
14. Wang Y, Yang G, Gong J, Lu F, Diao Q, Sun J, Zhang K, Tian J and Liu J: Ginseng for Alzheimer's Disease: A systematic review and meta-analysis of randomized controlled trials. Curr Top Med Chem 16: 529-536, 2016.
15. Zhang X, Wang Y, Ma C, Yan Y, Yang Y, Wang X and Rausch WD: Ginsenoside Rd and ginsenoside Re offer neuroprotection in a novel model of parkinson's disease. Am J Neurodegener Dis 5: 52-61, 2016.
16. Rai SN and Singh P: Advancement in the modelling and therapeutics of parkinson's disease. J Chem Neuroanat 104: 101752, 2020.
17. Liu M, Bai X, Yu S, Zhao W, Qiao J, Liu Y, Zhao D, Wang J and Wang S: Ginsenoside Re inhibits ROS/ASK-1 dependent mitochondrial apoptosis pathway and activation of Nrf2-antioxidant response in beta-Amyloid-challenged SH-SY5Y cells. Molecules 24: 2687, 2019.
18. Livak KJ and Schmittgen TD: Analysis of relative gene expression data using real-time quantitative PCR and the 2(-Delta Delta C(T)) method. Methods 25: 402-408, 2001
19. Liu M, Yu S, Wang J, Qiao J, Liu Y, Wang S and Zhao Y: Ginseng protein protects against mitochondrial dysfunction and neurodegeneration by inducing mitochondrial unfolded protein response in Drosophila melanogaster PINK1 model of parkinson's disease. J Ethnopharmacol 247: 112213, 2020.
20. Ahmad S, Hussain A, Ullah F, Jamil M, Ali A, Ali S and Luo Y: 60Co-γ radiation alters developmental stages of zeugodacus cucurbitae (Diptera: Tephritidae) through apoptosis pathways gene expression. J Insect Sci 21: 16, 2021.
21. Ramalingam M, Huh Y and Lee Y: The impairments of α-Synuclein and mechanistic target of rapamycin in rotenone-induced SH-SY5Y cells and mice model of parkinson's disease. Front Neurosci 13: 1028, 2019.
22. Ren TT, Yang JY, Wang J, Fan SR, Lan R and Qin XY: Gisenoside Rg1 attenuates cadmium-induced neurotoxicity in vitro and in vivo by attenuating oxidative stress and inflammation. Inflamm Res 70: 1151-1164, 2021.
23. Xu C, Wu A, Zhu H, Fang H, Xu L, Ye J and Shen J: Melatonin is involved in the apoptosis and necrosis of pancreatic cancer cell line SW-1990 via modulating of Bcl-2/Bax balance. Biomed Pharmacother 67: 133-9, 2013.
24. Yatchenko Y and Ben-Shachar D: Update of mitochondrial network analysis by imaging: Proof of technique in schizophrenia. Methods Mol Biol 2277: 187-201, 2021.
25. Zorova LD, Demchenko EA, Korshunova GA, Tashlitsky VN, Zorov SD, Andrianova NV, Popkov VA, Babenko VA, Pevzner IB Silachev DN, *et al*: Is the mitochondrial membrane potential (ΔΨ) correctly assessed? Intracellular and intramitochondrial modifications of the ΔΨ probe, Rhodamine 123. Int J Mol Sci 23: 482, 2022.
26. Pessoa J: Live-cell visualization of cytochrome c: A tool to explore apoptosis. Biochem Soc Trans 49: 2903-2915, 2021.
27. Chehade H, Fox A, Mor GG and Alvero AB: Determination of caspase activation by western blot. Methods Mol Biol 2255: 1-12, 2021.
28. Yüksel M, Nazıroğlu M and Özkaya MO: Long-term exposure to electromagnetic radiation from mobile phones and Wi-Fi devices decreases plasma prolactin, progesterone, and estrogen levels but increases uterine oxidative stress in pregnant rats and their offspring. Endocrine 52: 352-362, 2016.
29. Shahcheraghi SH, Salemi F, Peirovi N, Ayatollahi J, Alam W, Khan H and Saso L: Nrf2 regulation by curcumin: Molecular aspects for therapeutic prospects. Molecules 28: 167, 2021.
30. Kanno T, Tanaka K, Yanagisawa Y, Yasutake K, Hadano S, Yoshii F, Hirayama N and Ikeda JE: A novel small molecule, N-(4-(2-pyridyl) (1,3-thiazol-2-yl))-2-(2,4,6-trimethylphenoxy) acetamide, selectively protects against oxidative stress-induced cell death by activating the Nrf2-ARE pathway: Therapeutic implications for ALS. Free Radic Biol Med 53: 2028-2042, 2012.
31. Liu X, Wang C, Liu W, Song S, Fu J, Hayashi T, Mizuno K, Hattori S, Fujisaki H and Ikejima T: Oral administration of silibinin ameliorates cognitive deficits of parkinson's disease mouse model by restoring mitochondrial disorders in hippocampus. Neurochem Res 46: 2317-2332, 2021.
32. Li Y, Tang J, Khatibi NH, Zhu M, Chen D, Tu L, Chen L and Wang S: Treatment with ginsenoside rb1, a component of panax ginseng, provides neuroprotection in rats subjected to subarachnoid hemorrhage-induced brain injury. Acta Neurochir Suppl 110: 75-79, 2011.
33. Chen X, Zhang Z, Li H, Zhao J, Wei X, Lin W, Zhao X, Jiang A, Yuan J: Endogenous ethanol produced by intestinal bacteria induces mitochondrial dysfunction in non-alcoholic fatty liver disease. J Gastroenterol Hepatol 35: 2009-2019, 2020.
34. Gibson GE, Kingsbury AE, Xu H, Lindsay JG, Daniel S, Foster OJ, Lees AJ and Blass JP: Deficits in a tricarboxylic acid cycle enzyme in brains from patients with parkinson's disease. Neurochem Int 43: 129-135, 2003.
35. Ahn EH, Lei K, Kang SS, Wang ZH, Liu X, Hong W, Wang YT, Edgington-Mitchell LE, Jin L and Ye K: Mitochondrial dysfunction triggers the pathogenesis of parkinson's disease in neuronal C/EBP β transgenic mice. Mol Psychiatry 26: 7838-7850, 2021.
36. Shi J, Xue W, Zhao WJ and Li KX: Pharmacokinetics and dopamine/acetylcholine releasing effects of ginsenoside Re in hippocampus and mPFC of freely moving rats. Acta Pharmacol Sin 34: 214-220, 2013.
37. Espinosa-Oliva AM, García-Revilla J, Alonso-Bellido IM and Burguillos MA: Brainiac caspases: Beyond the wall of apoptosis. Front Cell Neurosci 13: 500, 2019.
38. Madhi I, Kim JH, Shin JE and Kim Y: Ginsenoside Re exhibits neuroprotective effects by inhibiting neuroinflammation via CAMK/MAPK/NF-κB signaling in microglia. Mol Med Rep 24: 698, 2021.
39. Yang X, Chu SF, Wang ZZ, Li FF, Yuan YH and Chen NH: Ginsenoside Rg1 exerts neuroprotective effects in 3-nitropronpionic acid-induced mouse model of Huntington's disease via suppressing MAPKs and NF-κB pathways in the striatum. Acta Pharmacol Sin 42: 1409-1421, 2021.
40. Liu Y, Yu S, Xing X, Qiao J, Yin Y, Wang J, Liu M and Zhang W: Ginsenoside Rh2 stimulates the production of mitochondrial reactive oxygen species and induces apoptosis of cervical cancer cells by inhibiting mitochondrial electron transfer chain complex. Mol Med Rep 24: 873, 2021.
41. Ilie OD, Ciobica A, McKenna J, Doroftei B and Mavroudis I: Minireview on the relations between Gut microflora and parkinson's disease: Further biochemical (oxidative stress), inflammatory, and neurological particularities. Oxid Med Cell Longev 2020: 4518023, 2020.
42. Li Q, Qiu Z, Wang Y, Guo C, Cai X, Zhang Y, Liu L, Xue H and Tang J: Tea polyphenols alleviate hydrogen peroxide-induced oxidative stress damage through the Mst/Nrf2 axis and the Keap1/Nrf2/HO-1 pathway in murine RAW264.7 cells. Exp Ther Med 22: 1473, 2021.

43. Terada K, Murata A, Toki E, Goto S, Yamakawa H, Setoguchi S, Watase D, Koga M, Takata J, Matsunaga K and Karube Y: Atypical antipsychotic drug ziprasidone protects against rotenone-induced neurotoxicity: An in vitro study. Molecules 25: 4206, 2020.
44. He YB, Liu YL, Yang ZD, Lu JH, Song Y, Guan YM and Chen YM: Effect of ginsenoside-Rg1 on experimental parkinson's disease: A systematic review and meta-analysis of animal studies. Exp Ther Med 21: 552, 2021.
45. Han Y, Wang T, Li C, Wang Z, Zhao Y, He J, Fu L and Han B: Ginsenoside Rg3 exerts a neuroprotective effect in rotenone-induced parkinson's disease mice via its anti-oxidative properties. Eur J Pharmacol 909: 174413, 2021.